PCCP

PAPER

View Article Online
View Journal | View Issue

Cite this: *Phys. Chem. Chem. Phys.*, 2023, **25**, 22662

Accurate absolute frequency measurement of the S(2) transition in the fundamental band of H_2 near 2.03 μm

D. Mondelain,* L. Boux de Casson, H. Fleurbaey, S. Kassi and A. Campargue

Received 6th July 2023,
Accepted 26th July 2023

DOI: 10.1039/d3cp03187j

rsc.li/pccp

A series of spectra of the quadrupolar electric S(2) transition of H_2 in the 1–0 band near 4917 cm^{-1} has been recorded at seven pressure values between 2 and 100 Torr. The comb-referenced cavity ring down spectroscopy (CR-CRDS) technique was used for the recording of this very weak transition. The accuracy of the spectrum frequency axis is achieved by linking the CRDS setup to an optical frequency comb referenced to a GPS-referenced 10 MHz rubidium clock. Applying a multi-spectrum fit procedure to the seven averaged spectra with a quadratic speed dependence Nelkin–Ghatak profile, the transition frequency is determined (ν_0 = 147 408 142 357 kHz) with an uncertainty of 150 kHz ($\sim 1 \times 10^{-9}$ in relative). This represents the smallest uncertainty achieved so far for a transition in the fundamental band of H_2. The experimental frequency reported in this work is 1.53 MHz higher than the best-to-date theoretical value. This difference represents 1.5 times the 1σ-uncertainty (about 1 MHz) of the calculated frequency. The measurements also allow for the determination of the absolute intensity value of the S(2) line which shows an agreement with the *ab initio* value at the per mil level. In addition, the cross section of the collision induced absorption (CIA) underlying the S(2) line is accurately retrieved from the quadratic pressure dependence of the baseline level of the recorded spectra.

1. Introduction

Di-hydrogen and its isotopologues are the simplest neutral molecular systems, and their rovibrational energy levels in the electronic ground state can be accurately determined by theoretical calculations.[1] To achieve a high degree of accuracy, these calculations include corrections to the Born–Oppenheimer approximation, as well as high order quantum electrodynamics (QED) corrections and finite nuclear size effects. A comparison of the theoretical values with accurate experimental measurements provides a strong test of the QED theory which fully describes the molecular systems and puts a higher limit on the coupling strength of a potential 5th force.[2,3] Because H_2 and D_2 are homonuclear molecules, their ro-vibrational absorption spectrum consists of only very weak electric-quadrupole transitions. This results in a real experimental challenge to measure the absolute frequency of such weak transitions with accuracy competing with that reported for the theoretical value. As an example, the strongest transition in the 1–0 fundamental band of H_2 has a line intensity of 3.2×10^{-26} cm molecule^{-1} at 296 K[4] and the minimal required uncertainty should be below 1 MHz. Thanks to the presence of a weak electric dipole moment, the HD isotopologue possesses transitions which are stronger than the H_2 and D_2 quadrupolar transitions, making it a better choice for metrological frequency determination. Nevertheless, to check the potential (vibrational, isotopologue) dependence of the *ab initio* calculations, it is important to have at disposal the largest number of accurate experimental frequency measurements as possible for different isotopologues, vibrational bands and transitions. Up to now, such measurements were relatively scarce (ref. 5, 6 and references herein). Most of them were obtained by Doppler limited spectroscopy. Saturation spectroscopy has been applied to HD transitions but with the drawback of an hyperfine structure limiting the final accuracy on the line centre determination.[7–11] Very recently, Cozijn and co-workers achieved a feat in saturating the S(0) transition in the 2–0 band of H_2 using the NICE-OHMS technique and a H_2 gas sample at 72 K[12] and reported a transition frequency uncertainty of 8 kHz, in agreement with the frequency measured with a 60 kHz uncertainty in the Doppler regime by comb-referenced cavity ring down spectroscopy (CR-CRDS).[5] This latter work, also including the frequency determination of five other transitions in the 2–0 band, evidenced a systematic underestimation of about 2.58 MHz of the most recent calculated H_2 frequencies, about twice their claimed uncertainties. Apart from these six

Univ. Grenoble Alpes, CNRS, LIPhy, Bat. E, 140 rue de la Physique, 38400 Saint-Martin d'Hères, France. E-mail: didier.mondelain@univ-grenoble-alpes.fr

transition frequencies measured with a sub-MHz uncertainty in the 2–0 band, only the Q(1) transition in the 1–0 band has been measured with such a level of accuracy.[6] The Q(1) 1–0 transition frequency near 4155 cm^{-1} was very recently reported with an uncertainty of 310 kHz using stimulated Raman scattering metrology.[6] The measured value was found to be 0.84 MHz larger than predicted by theory. In order to extend the measurements in the 1–0 fundamental band, we consider here the S(2) transition (ν_0 = 4917.006312 cm^{-1};[4] S = 4.577 × 10^{-27} cm $molecule^{-1}$).[13] The S(2) transition frequency is presently derived from a series of spectra recorded using a CRDS spectrometer referenced to an optical frequency comb (OFC). The setup and the acquisition procedure are detailed in the next section, followed by a description of the adopted multi-spectrum fit procedure (Section 3) and the budget error (Section 4). The retrieved absolute frequency and line shape parameters are then discussed and compared to previous works before concluding remarks (Section 5).

2. Setup and acquisition procedure

2.1. Experimental setup

A comb-referenced cavity ring down spectrometer used in this work is identical to the one described in ref 14. Briefly, it consists of an extended cavity diode laser (ECDL) which is coupled to a temperature stabilized high finesse cavity (TS-HFC).[15,16] The cavity is made of two high reflectivity mirrors (with a reflection coefficient of $R > 99.99\%$ over the 1950–2250 nm range) separated by 45.5 cm. Periodic resonances between the laser light and a cavity mode are achieved by applying a voltage triangular ramp on the PZT tube on which the output cavity mirror is installed. At each resonance, ring-down (RD) events are detected using a photodiode after switching off the injection of photons with an acousto-optic modulator (AOM). The ring down time at frequency ν, $\tau(\nu)$, is derived from a fit of the RD event with a purely decreasing exponential function. The extinction coefficient, $\alpha(\nu)$, is thus retrieved using eqn (1):

$$\alpha(\nu) = \frac{n}{c\tau(\nu)} - \frac{1 - R(\nu)}{L_{cav}} \quad (1)$$

where c is the speed of light, n is the refractive index of the absorbing gas, $R(\nu)$ is the reflectivity of the mirrors and L_{cav} is the cavity length. Typical RD time of the evacuated cell is $\tau \sim 51$ μs at 4917 cm^{-1}.

The rest of the ECDL light is mixed with the output of an OFC to obtain a beat note (BN) signal detected using a fast photodiode. After acquisition of the signal, the beat note frequency, f_{BN}, is derived allowing retrieving the absolute frequency associated with the RD event from eqn (2):

$$\nu = nf_{rep} + f_{CEO} + f_{BN} - f_{AOM} \quad (2)$$

where the repetition rate, f_{rep} = 250 MHz, and the carrier-envelop offset, f_{CEO} = −20 MHz, of the OFC are referenced to a 10 MHz rubidium frequency standard phase-locked to a GPS timing receiver. The sinusoidal wave of frequency f_{AOM} = 94.15 MHz applied to the AOM is generated using a direct digital synthesizer (DDS) also referenced to the 10 MHz frequency standard as well as the fast BN acquisition board. Note that the minus sign for f_{AOM} is due to the fact that a beam of order of −1 is used. The tooth number, n, is determined using a commercial wavelength meter (HighFinesse WS7-60 IR-II). At the end, an absolute frequency known with an uncertainty of ∼200 kHz is associated with each RD event.

2.2. Acquisition procedure

Spectra are recorded step-by-step over a 0.3 cm^{-1} interval around the H_2 line with a typical spectral sampling of 5 × 10^{-3} cm^{-1}. The laser tuning is achieved by changing the voltage applied to the piezoelectric transducer (PZT) inside the ECDL. At each spectral step, the frequency of the laser source is smoothly stabilized thanks to the measured BN frequency and 200 RD events are acquired. About 20 minutes are necessary to record one spectrum under these conditions. A homemade software is then used to average the RD times and associated absolute frequencies, for each spectral step. A flow of high purity H_2 is established in the TS-HFC (Alphagaz 2 from Air Liquide; 99.9999% of purity) to limit the water vapour volume mixing ratio (Table 1). Indeed, the 8_{35}–9_{54} transition of the $\nu_2 + \nu_3$ band of $H_2{}^{16}O$ (ν_0 = 4916.9468 cm^{-1}; S = 8.097 × 10^{-25} cm $molecule^{-1}$)[4] is slightly interfering with the studied H_2 line. The pressure inside the cell is measured using either a heated absolute capacitance manometer (Model AA02A Baratron from MKS; 1000 mbar full scale; accuracy better than 0.12% of the reading) or an absolute capacitance manometer (Model AA01A Baratron from MKS; 10 mbar full scale; accuracy better than 0.25% of the reading) (Table 1). The pressure is regulated using an electro-valve (2871 series from Burkert; 0.3 mm orifice dia.) and a homemade PID software. A series of single spectra recorded for 7 pressure values ranging from

Table 1 Experimental conditions for different series of spectra of the S(2) 2–0 line of H_2

P_{tot} (Torr)	2	5	10	20	50	75	100
# Spectra	61	30	55	18	17	57	22
QF[a]	342	515	1350	1604	2599	3419	4067
RMS (cm^{-1})	2.0 × 10^{-11}	3.3 × 10^{-11}	2.5 × 10^{-11}	4.2 × 10^{-11}	6.6 × 10^{-11}	7.8 × 10^{-11}	8.9 × 10^{-11}
VMR_{H2O}[b] (ppm)	325.4	129.4	130.8	71.8	54.2	51.4	21.7
Pressure gauge[c]	Gauge #1	Gauge #1	Gauge #2	Gauge #2	Gauge #2	Gauge #2	Gauge #2
Temp. (K)	297.42	297.41	297.41	297.46	297.46	297.40	297.42

[a] QF (quality factors) correspond to the ratio of the absorption at the peak to the RMS of the residuals obtained with a qSDNG profile. [b] VMR: volume mixing ratio. [c] Gauge #1 : 10 mbar full scale; Gauge #2 : 1000 mbar full scale.

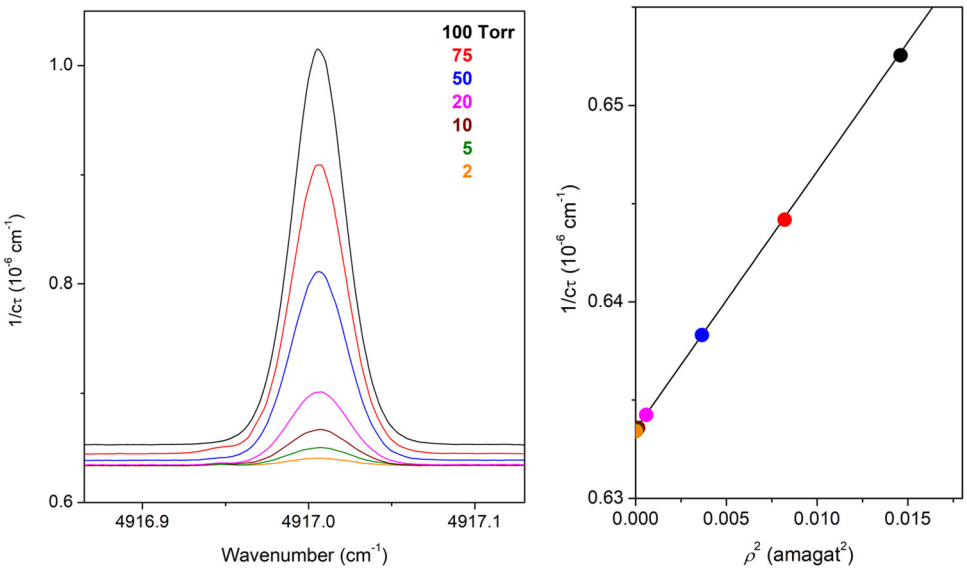

Fig. 1 Overview of the CRDS spectra recorded for the S(2) transition at different pressures (left panel). Note the increase of the spectrum baseline with the squared density, ρ^2, due to collisional induced absorption (CIA) of H_2 measured at 4916.860 cm^{-1} (right panel).

2 Torr to 100 Torr are displayed in Fig. 1. The temperature measured with an accuracy of 0.04 K was maintained at an almost constant value of 297.43(3) K. Note that on Fig. 1, we clearly observe that the baseline level of the spectra increases with the pressure (or density) squared due to the underlying collision induced absorption (CIA). The corresponding CIA cross-section will be derived below using the baseline determined during the fit of the S(2) line profile.

All the spectra recorded for the same pressure value (between 17 and 61 – see Table 1) were merged together and averaged by bins. More precisely, over each equally spaced bin of 0.002 cm^{-1}, a mean value is calculated for the frequency and the loss rate, $1/c\tau$. As a result, seven averaged spectra are obtained for the multi-spectrum fit procedure described below.

3. Multispectrum fit procedure

The frequency of the S(2) transition, ν_0, is determined from a multi-spectrum fit procedure using the Multi-spectrum Analysis Tool for Spectroscopy (MATS) fitting program developed at NIST.[17] This procedure is applied to the seven averaged spectra corresponding to the seven pressure values between 2 and 100 Torr. Two different line profiles have been tested:

(i) A quadratic speed-dependent Nelkin–Ghatak (qSDNG) profile[18] which takes into account the Doppler effect, the collision-induced velocity changes (or Dicke narrowing), quantified by the velocity changing collision rate, ν_{VC}, the collisional broadening and shift and their quadratic speed-dependence. In this profile, the parameter, η, describing the correlation between velocity and internal-state changes in the Hartmann Tran (HT) profile is fixed to zero.

(ii) A β-qSDNG profile[19,20] for which the Dicke narrowing is treated with an approximation of the billiard ball model[21] including the mass ratio of colliding molecules and the relative importance of speed- and direction-changing collision. This latter profile is supposed to better model molecular systems with large Dicke narrowing such as H_2 and its isotopologues.[19]

The qSDNG profile is characterized by the transition frequency at zero pressure, ν_0, the line-broadening and pressure-shift coefficients (γ_0 and δ_0, respectively), the Dicke narrowing parameter (ν_{VC}/P_{tot}), the speed dependence of the pressure-broadening (γ_2) and the pressure-shift (δ_2) (all in cm^{-1} atm^{-1}). In the β-qSDNG profile, ν_{VC} is replaced by $\beta(\chi)\nu_{VC}$, where β is a correction depending of $\chi = \nu_{VC}/\Gamma_D$. Γ_D is the Doppler width which is fixed to its value calculated at the measured temperature. During the fitting procedure, the mole fraction of H_2 is fixed to 1 while the integrated intensity of the S(2) transition is fitted independently for each pressure together with a linear baseline. As already mentioned, it is necessary to consider the interfering water vapour absorption lines in the fit and especially the 8_{35}–9_{54} transition of $H_2{}^{16}O$ at ν_0 = 4916.9468 cm^{-1} with a line intensity $S = 8.097 \times 10^{-25}$ cm molecule^{-1},[4] and the other water interfering lines which are at least two orders of magnitude weaker. For this, the water vapour volume mixing ratio (reported in Table 1) the position, pressure-broadening and pressure-shift coefficients of the strongest water transition are fitted.

The results of the multi-spectrum fit procedure obtained with different profiles are illustrated in Fig. 2 and the retrieved parameters are reported in Table 2. Residuals exceeding the noise level are observed if the speed-dependence of the pressure-shift is not considered, $\delta_2 = 0$, when using a qSDNG profile. Improved residuals, but still above the noise level for the four highest pressures, are obtained for both the qSDNG and β-qSDNG profiles with δ_2 fitted. In contrast to what could be expected, the latter profile shows no real improvement of the residuals compared to the qSDNG profile: residuals are slightly

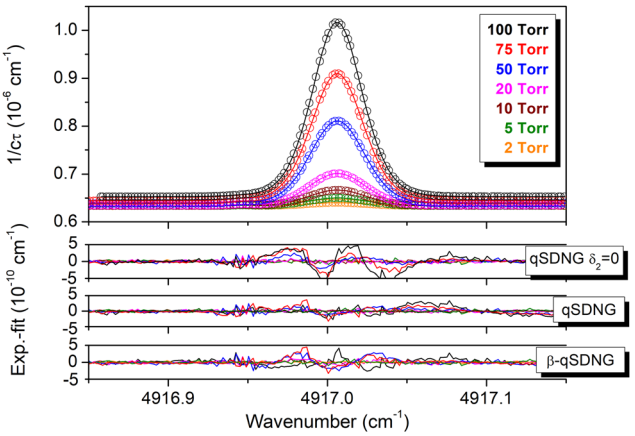

Fig. 2 Upper panel: CRDS spectra of the S(2) transition of H_2 in the 1–0 band recorded at seven pressure values. Lower panels: corresponding (exp.-fit) residuals obtained after the multi-spectrum fit procedure using the qSDNG and β-qSDNG profiles.

better at 100 Torr but larger at 50 and 20 Torr and equivalent for the other pressures. This leads to quality factors between 4067 for the 100 Torr spectrum and 342 for the 2 Torr spectrum (Table 1) with the qSDNG profile.

In addition, the CIA can be extracted from the baselines obtained using the multi-spectrum fit procedure. For this purpose, the loss rate, $1/c\tau$, corresponding to the baseline value for the 4916.860 cm^{-1} wavenumber, is plotted *versus* the squared density in amagat^2 (Fig. 1, right panel) and then fitted with a linear function. The retrieved slope $(1.310(4) \times 10^{-6}$ cm^{-1} amagat^{-2}) at 4916.86 cm^{-1} and 297.43 K is very close (0.7%) to the (calculated) value of 1.319×10^{-6} cm^{-1} amagat^{-2} reported in the HITRAN2020 database[4] at 4917.00 cm^{-1} and 300 K.

4. Budget error

More important than the fit residuals is the statistical uncertainty on the retrieved ν_0 value for different profiles and the dependence of ν_0 to the choice of the profile. As can be seen from Table 2, the retrieved ν_0 value varies by no more than 6×10^{-7} cm^{-1} (18 kHz) between the β-qSDNG and qSDNG profiles, largely within the statistical uncertainty given by the fit (between 100 and 170 kHz according to the profile). The limited impact of the choice of the profile on ν_0 has already been discussed in the study of the (2–0) transitions in ref. 5. In addition, we see in Table 2 (as in ref. 5) that the δ_2 value has a very limited impact on the retrieved ν_0 value.

In ref. 23, it was shown that the uncertainty on the frequency due to the optical frequency comb, the Doppler shift induced by the moving speed of the output mirror of the optical cavity and the AC/DC Stark shifts are well below the kHz level.

As mentioned in ref. 24, *the off-diagonal elements relat(ing) to the numerical correlation between floated parameters in the fit, (...) are not used in calculation of the standard error* leading to the possible underestimation of the «real error». To estimate if this is the case here, we first simulated 100 sets of seven spectra with different random noises and then calculated the standard deviation of the retrieved ν_0 frequency from the multi-spectrum fit procedure. Under the typical noise conditions of our recordings (10 kHz on the *x*-axis and 5×10^{-11} cm^{-1} on the *y*-axis), we found that the uncertainty given by the fit for ν_0 (and for δ_0 and δ_2 too) is representative of the « real error ».

We also evaluated the impact on ν_0 of the uncertainty given by the fit procedure for δ_0 and δ_2 which are the two parameters which are significantly correlated with ν_0. The fit procedure was run twice: the first one with δ_0 or δ_2 fixed to their fitted values and the second time by fixing them to their fitted values increased by the fit uncertainty. We obtained a variation of 3.0×10^{-6} cm^{-1} ($\approx$ 90 kHz) on ν_0 for δ_0 and that of 1.8×10^{-6} cm^{-1} ($\approx$ 48 kHz) for δ_2. Note that in the MATS program, $a_s = \delta_0/\delta_2$ is the parameter which is fitted instead of δ_2 directly.

We proceeded in the same way to evaluate the impact of an error on the position, pressure-broadening and pressure-shift coefficients of the interfering water transition. The fit uncertainty on ν_{0_H2O}, $\gamma_{0\text{-}H2O}$ and δ_{0_H2O} propagates to uncertainties of 3.3×10^{-7} cm^{-1}, 2.3×10^{-7} cm^{-1} and 7.4×10^{-7} cm^{-1} on ν_0, respectively. The retrieved values for ν_{0_H2O}, $\gamma_{0\text{-}H2O}$ and δ_{0_H2O} are 4916.94687(8) cm^{-1}, 0.0591(11) cm^{-1} atm^{-1} and −0.0074(11) cm^{-1} atm^{-1}, respectively. The position value is very close to the value included in the HITRAN2020 database

Table 2 Line shape parameters of the S(2) transition obtained from the multi-spectrum treatment of the CRDS spectra recorded at seven pressure values using the β-qSDNG and qSDNG profiles. The uncertainties given within parenthesis in the unit of the last quoted digit correspond to the (1σ) statistical values provided by the fit. The *ab initio* absolute frequency value given for the S(2) transition by the H2spectre software,[22] and the *ab initio* line shape parameters and measured absolute frequency provided in ref. 6 for the Q(1)(1–0) transition are also listed for comparison

	ν_0 cm^{-1}	γ_0 10^{-4} cm^{-1} atm^{-1}	δ_0 10^{-3} cm^{-1} atm^{-1}	ν_{VC}/P_{tot} 10^{-2} cm^{-1} atm^{-1}	γ_2 10^{-4} cm^{-1} atm^{-1}	δ_2 10^{-3} cm^{-1} atm^{-1}
Ab initio	4917.006312(33)					
β-qSDNG	4917.0063643(41)	11.8(7)	−1.05(4)	1.87(2)	1.25(7)	1.82(11)
qSDNGP	4917.0063637(32)	10.6(6)	−1.04(3)	1.24(1)	1.03(11)	1.76(13)
qSDNGP (δ_2= 0)	4917.0063651(56)	10.3(9)	−1.56(5)	1.25(2)	0.96(16)	0
Recommended value	4917.006363(5)[a]					
Ref. 6	4155.253790(10)	6.4(6)	−1.17(12)	4.31(21)	1.06(10)	2.30(22)

[a] The recommended value is corrected from the recoil and second-order Doppler shifts. The uncertainty includes all the uncertainty sources discussed in the budget error section.

(with a difference of 7×10^{-5} cm^{-1}). The pressure broadening and the pressure-shift coefficients of the considered H_2O line by H_2 are in agreement within the error bars with the values calculated in ref. 25 and 26 using the Modified Complex Robert-Bonamy (MCRB) formalism (0.0695(139) cm^{-1} atm^{-1} and $-0.0082(5)$ cm^{-1} atm^{-1}, respectively).

It is also necessary to mention that the R(17)e transition of $^{12}C^{18}O^{16}O$ in the 20012–00001 band (ν_0 = 4916.969519 cm^{-1} and $S = 2.431 \times 10^{-24}$ cm molecule^{-1})[4] is a potential interfering line. To evaluate its potential impact on ν_0, we looked for the possible traces of CO_2 in the sounded gas by recording the spectra of the stronger P(60) $^{12}C^{16}O_2$ line (ν_0 = 4918.07704 cm^{-1} and $S = 7.37 \times 10^{-24}$ cm molecule^{-1}) of the 20012–00001 band. No absorption due to this line was observed in our spectra giving an upper limit of 0.25 ppm for the CO_2 mixing ratio in our sample. Neglecting the potential presence of 0.25 ppm of CO_2 in our cell (at all pressure values) leads to a bias of 1.7×10^{-6} cm^{-1}.

The fitted value of ν_0 needs to be corrected from the recoil shift,[27] leading to a reduction of the frequency by −23.9 kHz in our case, and the second-order Doppler shift[28] corresponding to an almost negligible shift of +1 kHz. The recommended absolute wavenumber of the S(2) transition is reported in Table 2 with a final uncertainty of 5×10^{-6} cm^{-1} (*i.e.* 150 kHz) corresponding to the quadrature sum of all the different contributions described above.

As can be observed in Fig. 2, residuals are not at the noise level for the highest pressures, showing some limitations of the qSDNGP model. To overcome these limitations and evaluate the impact of the highest-pressure spectra, we removed the 100, 75 and 50 Torr averaged spectra from the multi-fit procedure keeping only the 2, 5, 10 and 20 Torr spectra for the fit. The retrieved ν_0 values in both cases are very close to each other: a difference of 1×10^{-6} cm^{-1} with a qSDNG profile and 2.4×10^{-6} cm^{-1} with a β-qSDNG profile were observed, largely within an uncertainty of 1×10^{-5} cm^{-1} provided by the fit of the four lowest pressure spectra. In other words, including the highest pressure spectra allows improving the fit uncertainty but does not impact the retrieved ν_0 value.

5. Discussion and concluding remarks

When comparing the *ab initio* values reported in ref. 6 for the Q(1) transition in the 1–0 band of H_2 with the fitted line profile parameters obtained for a β-qSDNG profile (Table 2), we notice that δ_0, γ_2 and δ_2 parameters are close but the ν_{VC}/P_{tot} *ab initio* value is two times larger than our fitted value. This large difference could be due to the fact that a slightly different profile, including an imaginary part for ν_{VC}, is used in ref. 6. Finally, the γ_0 *ab initio* value is about two times smaller than our retrieved value. This could be due to the fact that these two transitions do not involve the same J values. As observed in ref. 20,29, J-dependence exists for γ_0. Indeed, the γ_0 value retrieved for the Q(1) transition is clearly smaller than those reported for other Q transitions measured by Raman spectroscopy in ref. 29.

Even though it was not the initial goal of this work, it is interesting to mention that the integrated intensity of the S(2) transition at 296 K, retrieved from the spectra recorded at the different pressures, show values between 4.567×10^{-27} and 4.579×10^{-27} cm molecule^{-1} (if we except the 10 Torr spectrum for which the pressure value measured with the 1000 mbar gauge leads to a clear outlier with a value of 4.594×10^{-27} cm molecule^{-1}). The mean value of $4.572(2) \times 10^{-27}$ cm molecule^{-1} confirms the *ab initio* intensity value included in the HITRAN database (4.577×10^{-27} cm molecule^{-1}) at the per mil level.

In summary, in this work, a series of spectra obtained using a highly sensitive CRDS spectrometer linked to an optical frequency comb referenced to a rubidium atomic clock phase-locked to a GPS timing receiver have allowed the determination of the frequency of the S(2) transition (ν_0 = 147 408 142 357 kHz) with a final uncertainty of 150 kHz. Note that, to the best of our knowledge (see the review included in ref. 30), the detection of the considered S(2) 1–0 was not reported since the early works by Fink *et al.*[31] and Bragg *et al.*[32] using a grating spectrograph (1.4 km absorption path length) and a Fourier transform spectrometer (path length of 434 m and pressure values between 0.8 and 2.8 atm), respectively. With its 150 kHz final uncertainty, the reported transition frequency is the most accurate determination reported so far in the fundamental band of H_2, improving by more than two orders of magnitude the accuracy of these previous determinations. This is also two times smaller than the best uncertainty achieved in the fundamental band of H_2 (for the Q(1) transition which is 4.5 times stronger).[6]

The measured value of the S(2) transition frequency is 51×10^{-6} cm^{-1} (*i.e.* 1.53 MHz) higher than the *ab initio* value

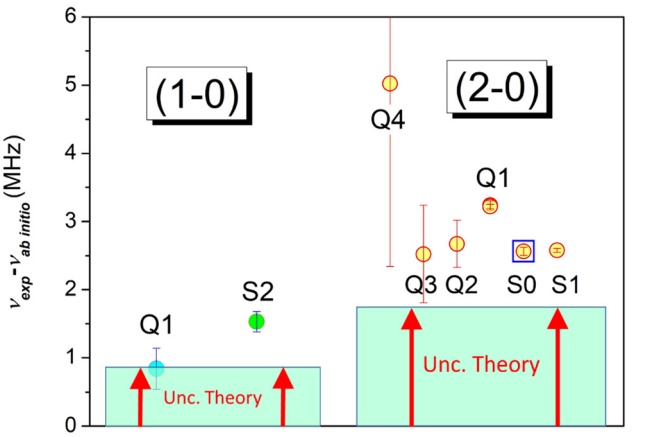

Fig. 3 Differences between the experiment and the theory for the H_2 transition frequencies of the 1–0 and 2–0 bands referenced to an absolute frequency standard. The theoretical values[1] were obtained from the H2spectre software.[22] The red arrows represent the typical uncertainty on the calculated values. The experimental values in the 1–0 band are from the study of Lamperti *et al.*[6] and this work (Q(1) and S(2), respectively) and from the study of Fleurbaey *et al.*[5] for the 2–0 band (yellow dots), the Lamb dip measurement of the S(0) 2–0 frequency is also indicated (blue open square).[12]

obtained using the H2spectre software V7.4.[22] This difference is 1.5 times larger than the 1σ-uncertainty reported in ref. 22 and confirms the fact that *ab initio* values are systematically smaller than experimental ones for H_2 and its isotopologues.[5,6,11] This tendency is illustrated in Fig. 3 which compares the H_2 transition frequencies of the 1–0 and 2–0 bands referenced to an absolute frequency standard to the best *ab initio* values.[22] Note that a smaller difference of 0.84 MHz (equivalent to the *ab initio* error bar) was found by Lamperti and co-workers[6] for the Q(1) transition belonging to the same 1–0 band of H_2 and given with a uncertainty of 310 kHz.

Conflicts of interest

There are no conflicts to declare.

Acknowledgements

The authors are grateful to F. Gibert from LMD and P. Cacciani from PhLAM for lending the thulium doped fiber amplifier and the external cavity diode laser, respectively.

References

1 J. Komasa, M. Puchalski, P. Czachorowski, G. Łach and K. Pachucki, Rovibrational energy levels of the hydrogen molecule through nonadiabatic perturbation theory, *Phys. Rev. A*, 2019, **100**, 032519.
2 W. Ubachs, J. C. J. Koelemeij, K. S. E. Eikema and E. J. Salumbides, Physics beyond the standard model from hydrogen spectroscopy, *J. Mol. Spectrosc.*, 2016, **320**, 1–12.
3 E. J. Salumbides, J. C. J. Koelemeij, J. Komasa, K. Pachucki, K. S. E. Eikema and W. Ubachs, Bounds on fifth forces from precision measurements on molecules, *Phys. Rev. D: Part., Fields, Gravitation, Cosmol.*, 2013, **87**, 112008.
4 I. E. Gordon, L. S. Rothman, R. J. Hargreaves, R. Hashemi, E. V. Karlovets, F. M. Skinner, E. K. Conway, C. Hill, R. V. Kochanov, Y. Tan, P. Wcisło, A. A. Finenko, K. Nelson, P. F. Bernath, M. Birk, V. Boudon, A. Campargue, K. V. Chance, A. Coustenis, B. J. Drouin, J.-M. Flaud, R. R. Gamache, J. T. Hodges, D. Jacquemart, E. J. Mlawer, A. V. Nikitin, V. I. Perevalov, M. Rotger, J. Tennyson, G. C. Toon, H. Tran, V. G. Tyuterev, E. M. Adkins, A. Baker, A. Barbe, E. Canè, A. G. Császár, A. Dudaryonok, O. Egorov, A. J. Fleisher, H. Fleurbaey, A. Foltynowicz, T. Furtenbacher, J. J. Harrison, J.-M. Hartmann, V.-M. Horneman, X. Huang, T. Karman, J. Karns, S. Kassi, I. Kleiner, V. Kofman, F. Kwabia–Tchana, N. N. Lavrentieva, T. J. Lee, D. A. Long, A. A. Lukashevskaya, O. M. Lyulin, V. Y. Makhnev, W. Matt, S. T. Massie, M. Melosso, S. N. Mikhailenko, D. Mondelain, H. S. P. Müller, O. V. Naumenko, A. Perrin, O. L. Polyansky, E. Raddaoui, P. L. Raston, Z. D. Reed, M. Rey, C. Richard, R. Tóbiás, I. Sadiek, D. W. Schwenke, E. Starikova, K. Sung, F. Tamassia, S. A. Tashkun, J. Vander Auwera, I. A. Vasilenko, A. A. Vigasin, G. L. Villanueva, B. Vispoel B, G. Wagner, A. Yachmenev and S. N. Yurchenko, The HITRAN2020 molecular spectroscopic database, *J. Quant. Spectrosc. Radiat. Transf.*, 2022, **277**, 107949.
5 H. Fleurbaey, A. O. Koroleva, S. Kassi and A. Campargue, The high-accuracy spectroscopy of H_2 rovibrational transitions in the (2-0) band near 1.2 μm, *Phys. Chem. Chem. Phys.*, 2023, **25**, 14749–14756.
6 M. Lamperti, L. Rutkowski, D. Ronchetti, D. Gatti, R. Gotti, G. Cerullo, F. Thibault, H. Jóźwiak, S. Wójtewicz, P. Masłowski, P. Wcisło, D. Polli and M. Marangoni, Stimulated Raman scattering metrology of molecular hydrogen, *Commun. Phys.*, 2023, **6**, 67.
7 F. M. J. Cozijn, P. Dupré, E. J. Salumbides, K. S. E. Eikema and W. Ubachs, Sub-Doppler frequency metrology in HD for test of fundamental physics, *Phys. Rev. Lett.*, 2018, **120**, 153002.
8 M. L. Diouf, F. M. J. Cozijn, B. Darquié, E. J. Salumbides and W. Ubachs, Lamb-dips and Lamb-peaks in the saturation spectrum of HD, *Opt. Lett.*, 2019, **44**, 4733.
9 M. L. Diouf, F. M. J. Cozijn, K.-F. Lai, E. J. Salumbides and W. Ubachs, Lamb-peak spectrum of the HD (2-0) P(1) line, *Phys. Rev. Res.*, 2020, **2**, 023209.
10 T.-P. Hua, Y. R. Sun and S.-M. Hu, Dispersion-like lineshape observed in cavity-enhanced saturation spectroscopy of HD at 1.4 μm, *Opt. Lett.*, 2020, **45**, 4863.
11 F. M. J. Cozijn, M. L. Diouf, V. Hermann, E. J. Salumbides, M. Schlösser and W. Ubachs, Rotational level spacings in HD from vibrational saturation spectroscopy, *Phys. Rev. A*, 2022, **105**, 062823.
12 F. M. J. Cozijn, M. L. Diouf and W. Ubachs, Lamb dip of a Quadrupole Transition in H_2, arXiv, preprint, arXiv:2303.17818v1.
13 L. Wolniewicz, I. Simbotin and A. Dalgarno, Quadrupole Transition Probabilities for the Excited Rovibrational States of H_2, *Astrophys. J., Suppl. Ser.*, 1998, **115**, 293–313.
14 D. Mondelain, A. Campargue, H. Fleurbaey, S. Kassi and S. Vasilchenko, Line shape parameters of air-broadened $^{12}CO_2$ transitions in the 2.0 μm region, with their temperature dependence, *J. Quant. Spectrosc. Radiat. Transfer*, 2023, **298**, 108485.
15 S. Kassi, S. Guessoum, J. C. A. Abanto, H. Tran, A. Campargue and D. Mondelain, Temperature dependence of the collision-induced absorption band of O_2 near 1.27 μm, *J. Geophys. Res. Atm.*, 2021, **126**, e2021JD034860.
16 S. Vasilchenko, T. Delahaye, S. Kassi, A. Campargue, R. Armante, H. Tran and D. Mondelain, Temperature dependence of the absorption of the R(6) manifold of the $2\nu_3$ band of methane in air in support of the MERLIN mission, *J. Quant. Spectrosc. Radiat. Transfer*, 2023, **298**, 108483.
17 **https://github.com/usnistgov/MATS**.
18 H. Tran, N. H. Ngo and J.-M. Hartmann, Efficient computation of some speed-dependent isolated line profiles, *J. Quant. Spectrosc. Radiat. Transfer*, 2013, **129**, 199–220.
19 M. Konefał, M. Słowiński, M. Zaborowski, R. Ciuryło, D. Lisak and P. Wcisło, Analytical-function correction to the Hartmann–Tran profile for more reliable representation

of the Dicke-narrowed molecular spectra, *J. Geophys. Res. Atm.*, 2020, **242**, 106784.

20 P. Wcisło, I. E. Gordon, H. Tran, Y. Tan, S.-M. Hu, A. Campargue, S. Kassi, D. Romanini, C. Hill, R. V. Kochanov and L. S. Rothman, The implementation of non-Voigt line profiles in the HITRAN database: H_2 case study, *J. Geophys. Res. Atm.*, 2016, **177**, 75–91.

21 R. Ciuryło, D. Shapiro, J. R. Drummond and A. May, Solving the line-shape problem with speed-dependent broadening and shifting and with Dicke narrowing. II, *Phys. Rev. A: At., Mol., Opt. Phys.*, 2002, **65**, 12502.

22 **https://qcg.home.amu.edu.pl/H2Spectre.html**.

23 H. Fleurbaey, P. Čermák, A. Campargue, S. Kassi, D. Romanini, O. Votava and D. Mondelain, $^{12}CO_2$ transition frequencies with kHz-accuracy by saturation spectroscopy in the 1.99–2.09 μm region, *Phys. Chem. Chem. Phys.*, 2023, **25**, 16319.

24 E. M. Adkins and J. T. Hodges, Assessment of the precision, bias and numerical correlation of fitted parameters obtained by multi-spectrum fits of the Hartmann-Tran line profile to simulated absorption spectra, *J. Quant. Spectrosc. Radiat. Transfer*, 2022, **280**, 108100.

25 C. L. Renaud, K. Cleghorn, L. Hartmann, B. Vispoel and R. R. Gamache, Line shape parameters for the H_2O–H_2 collision system for application to exoplanet and planetary atmospheres, *Icarus*, 2018, **306**, 275–284.

26 R. R. Gamache, B. Vispoel, C. L. Renaud, K. Cleghorn and L. Hartmann, Vibrational dependence, temperature dependence, and prediction of line shape parameters for the H_2O-H_2 collision system, *Icarus*, 2019, **326**, 186–196.

27 Z. D. Reed, B. J. Drouin and J. T. Hodges, Inclusion of the recoil shift in Doppler-broadened measurements of CO_2 transition frequencies, *J. Quant. Spectrosc. Radiat. Transfer*, 2021, **275**, 107885.

28 *Laser Spectroscopy: Experimental Techniques*, ed. W. Demtröder, Springer, 4th edn, 2008, vol. 2.

29 L. Rahn, R. Farrow and G. Rosasco, Measurement of the self-broadening of the H_2 Q (0-5) Raman transitions from 295 to 1000 K, *Phys. Rev. A: At., Mol., Opt. Phys.*, 1991, **43**, 6075–6088.

30 A. Campargue, S. Kassi, K. Pachucki and J. Komasa, The absorption spectrum of H_2: CRDS measurements of the (2-0) band, review of the literature data and accurate *ab initio* line list up to 35 000 cm^{-1}, *Phys. Chem. Chem. Phys.*, 2012, **14**, 802–815.

31 U. Fink, T. A. Wiggins and D. H. Rank, Frequency and intensity measurements on the quadrupole spectrum of molecular hydrogen, *J. Mol. Spectrosc.*, 1965, **18**, 384–395.

32 S. L. Bragg, J. W. Brault and W. H. Smith, Line positions and strengths in the H_2 quadrupole spectrum, *Astrophys. J.*, 1982, **263**, 999–1004.

